JOURNAL OF MATERIALS SCIENCE 23 (1988) 2093–2101

Microstructural investigation and indentation response of pressureless-sintered α- and β-SiC

R. H. J. HANNINK*, Y. BANDO, H. TANAKA, Y. INOMATA
National Institute for Research in Inorganic Materials, Namiki 1-1, Sakura-mura, Niihari-gun, Ibaraki 305, Japan

The microstructure and indentation response of pressureless-sintered α- and β-SiC were studied using a high-resolution electron microscope and analytical electron microscopy. The materials were manufactured with boron and carbon as sintering aids. It was found that the overall porosity of the materials was very low but a large number of carbon inclusions were present. X-ray diffraction revealed the fabricated β-SiC material was of the same 3C polytype as the initial starting powder; however, electron microscope observations indicated that the material contained a high density of faulting of the α-forms. High-resolution imaging of grain boundaries in these materials indicated that the boundaries were very clean, and when they contained an amorphous intergranular film it was at most 0.5 to 1 nm thick. The presence of boron was not detected. Deformation due to identation took several forms. Firstly, radial cracks extending from the corners of the indent suffered little hindrance from the matrix microstructure, such that transgranular fracture was the dominant mode. Secondly, the deformation zone beneath the indentations showed copious lattice microcracks with some preferred orientation during crack formation and propagation.

1. Introduction

Silicon carbide and silicon nitride based ceramics have gained considerable importance because of applications as engineering components in a number of diverse fields. Such components may be used in the area of energy production and conversion chemical industries and as machine tools. To become a viable contender in large-volume applications, economic fabrication methods must be available. Pressureless sintering, via the addition of sintering aids, has become a well-recognised and accepted economic fabrication route [1].

Sintering aids used for silicon carbide based materials take two forms; these are referred to as the lattice-soluble N and lattice-insoluble P types. In SiC these aids have taken the form of carbides, nitrides or phosphides, generally of the boride type, but they also include elemental aluminium, calcium, chromium, iron, lithium and yttrium (see for example [2–5]). The lattice-soluble p-types aluminium and boron are considered the more efficient. However, the most common and successful additions as sintering aids have been boron and carbon [6–11].

Whilst the sintering characteristics of boron and carbon additions to SiC are generally well reported [10–12], the actual densification process does not appear to be well understood [1, 9, 11, 12]. The main confusion is in whether a liquid phase is involved and to what extent each element contributes to sintering, powder purification and grain refining. To date little has been published to elucidate this confusion, and even the microstructural distribution of these elements is not clear (cf. [9, 11, 13]).

The strength and fracture properties of pressureless-sintered SiC are also well documented [1, 12–15]; however, the crack propagation and crack interactions in polycrystalline SiC matrices have not received appropriate attention.

In this paper we report our microstructural investigation using analytical transmission electron microscopy of α- and β-SiC produced by pressureless sintering with carbon and boron as sintering aids. In addition we examined the response of these materials to plastic deformation and fracture (cracking) introduced by indentation. The possible implications of our observations to the fracture behaviour of these materials is also discussed.

2. Experimental procedure

The α- and β-SiC samples, produced from powders comprising 6H and 3C polytypes, respectively, were prepared from commercial-grade SiC powders (Ibiden Co. Ltd, Japan). Pressureless sintering was carried out for 1 h at 2100° C in an atmosphere of pure argon gas. The sintering aid additions consisted of 0.67 wt % boron and 2 wt % carbon. The boron was added as metallic boron and the carbon was added as phenolic resin. The samples were originally prepared as 3 to 4 mm × 4 mm × 40 mm bars, the basic physical properties of which are presented in Table I.

Samples for high-resolution analytical transmission electron microscope (TEM) observation were prepared

* *Permanent address:* CSIRO, Division of Materials Science and Technology, Normanby Road, Clayton, Victoria 3168, Australia.

0022–2461/88 $03.00 + .12

by cutting slices from the bars and trepanning 3 mm diameter discs from the slices. These discs were then ground down to 70 μm and polished to a 1 μm diamond finish using a technique for polishing hard materials [16]. The polished surfaces were indented using a Vickers indenter, with an array of indents using either 100 or 200 gm ($\sim$1 or $\sim$2 N) load. These discs were then thinned to electron transparency using 5 kV argon ions. Thinning was carried out predominantly from the unindented surface. About 1 μm was removed from the indented surface after perforation. The samples were examined at 400 keV in a Jeol 4000FX electron microscope fitted with an electron energy-loss spectrometer and a TN5500 X-ray energy-dispersive spectrometer. High resolution image interpretation was carried out intuitively using images taken at Schezer focus.

Prior to ion-beam thinning the samples were also subjected to optical microscope examination, i.e. in the as-polished and etched condition (using Murakami's reagent).

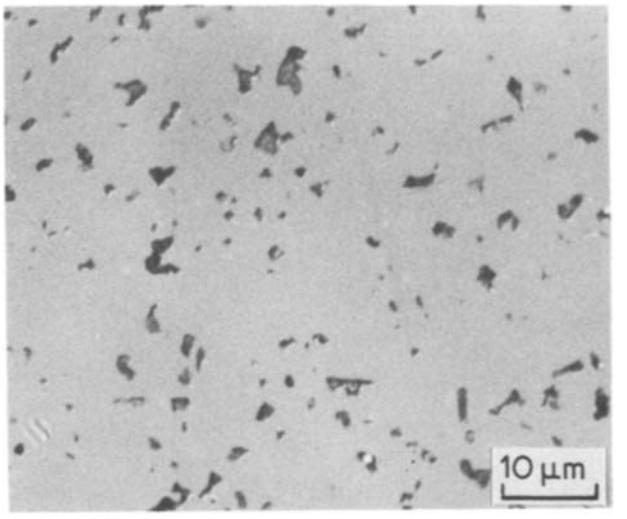

Figure 1 Optical micrograph of the as-polished surface of α-SiC showing inclusions and general lack of porosity.

3. Results and observations

3.1. Microstructural analyses

Optical microscope observations of the polished and unetched surfaces showed little porosity but a considerable amount of second phase. Both the α- and β-SiC samples showed this same microstructural feature. An optical microscope image of the as-polished surface of the α-SiC is shown in Fig. 1.

Etched surface and electron microscope (EM) microstructures of the α and β forms showed these materials to be quite dissimilar, as can be seen from the optical microscope images of Fig. 2. The α-SiC material had fairly equiaxed grains of about 7 μm (Fig. 2a) while the β-SiC material had a large proportion of tabular grains extending up to 10 μm in length (Fig. 2b). The average grain size in the β-SiC material was also about 7 μm, when the equiaxed grains were considered. The etched surface and EM observations also showed that the second phase observed in the unetched condition (Fig. 1) occurs in intergranular positions.

X-ray diffractometer traces of these samples indicated that the phase proportions had not altered measurably from that of the original starting materials, i.e. α-SiC predominantly 6H and β-SiC predominently 3C. However, the occurrence of tabular grains has always been associated with an α-SiC form (see for example [13]), and on this basis a considerable amount of α-type crystallography would be expected in the β-SiC sample. This was indeed the case when the β-SiC sample was examined in the electron microscope and studied using selected-area electron diffraction (SAED). When this procedure was used, 3C cubic-type grains were observed to contain copious faulting which showed the forms of the hexagonal 4H and 6H and rhombohedral 15R polytypes. Fig. 3a shows a typical non-tabular grain in the β-SiC material and from the selected-area electron diffraction pattern of this grain (Fig. 3b) it is evident that while the intense matrix spots show the 3C form the faulting was 6H. Evident from Fig. 3a is the heavily faulted nature of the grain; such faulting was one of the characteristic microstructural features of almost all the grains in the β-SiC material. After examining a considerable number of grains in the β-SiC sample, of both equiaxed and tabular form, it was concluded that less than 10% exhibited the 3C polytype in electron diffraction. The tabular grains, normally designated α-type, also displayed the 3C form with intense α-faulting. The apparent anomaly of these observations is discussed in more detail in Section 4.1.

Electron energy-loss spectroscopy (EELS) of the intergranular second-phase inclusions observed in the optical microscope revealed them to be composed of carbon. Fig. 4 shows the EELS spectrum of such an inclusion. In the spectrum we have indicated the positions of the Si_L and B_K edges. It is evident that these elements were not present in the inclusions. Further confirmation of the carbon pockets was obtained using SAED and high-resolution imaging. The ring pattern in Fig. 5a could be indexed as graphite (ASTM Card No. 23–65). The accompanying high-resolution electron microscope (HREM) image of Fig. 5b further

TABLE I Typical physical properties of pressureless-sintered α- and β-SiC

Material	Polytype	ϱ ($g\,cm^{-3}$)	E (GPa)	ν	H_V (GPa)	σ (MPa)	K_{Ic} ($MPa\,m^{1/2}$)
β-SiC [13]	3C	3.12	395	0.17	23	346*	2.8
α-SiC [14]	6H	3.07	381	0.16	20	500†	3.09
β-SiC [14]	3C	3.07	368	0.13	23	697†	3.44
β-SiC [15]	3C					650†	

*Four-point flexure test.
†Three-point flexure test.

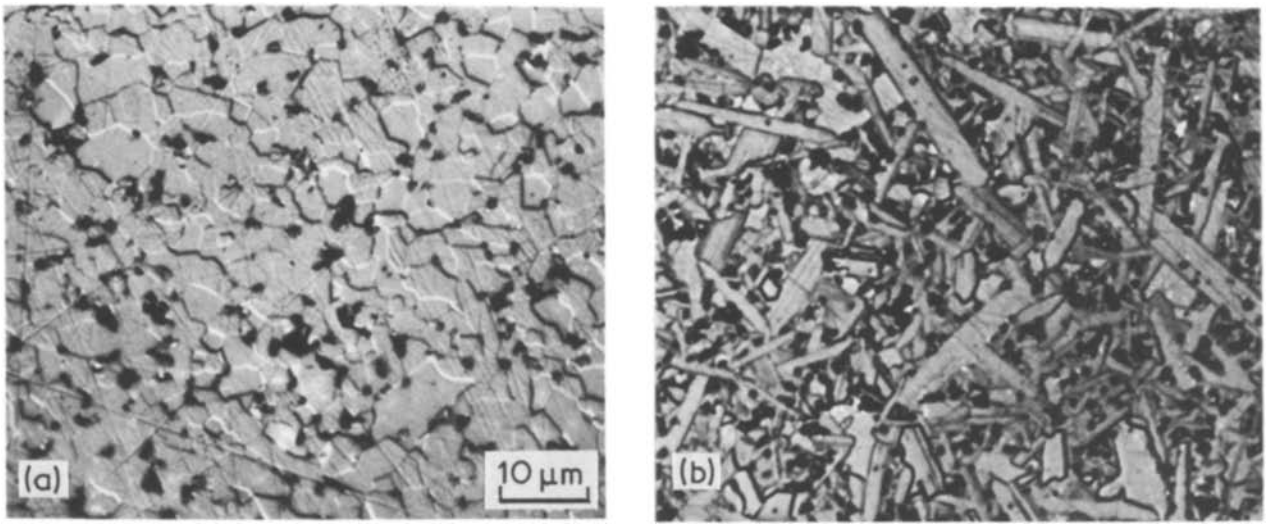

Figure 2 Grain morphology of (a) α-SiC and (b) β-SiC. Nomarski image of Murakami's reagent etched surface.

confirms the findings in that the graphite (0 0 2) fringes at 0.336 nm are clearly discernible.

Whilst the ring pattern in Fig. 5a was indexable as graphite, and was typical for a large number of measured inclusions, the much lower intensity of the (0 0 4) graphite reflection (normally $I/I_0 = 80$) could not be explained. This difference in intensity did not occur in single-crystal diffraction patterns obtained from graphite particles in the included agglomerates.

Other types of inclusions not containing boron were found in the intragranular positions, and a typical example is shown in Fig. 6. These inclusions were identified as containing either iron with chromium, manganese and molybdenum as minor elements, or as containing carbon. None of the observed inclusions contained boron. Further efforts were made to detect the presence of boron using both EELS and HREM imaging. Using these techniques the presence of boron could still not be established. For HREM examination a grain boundary was orientated such that one of the grains had the major diffracting vector of the ⟨1 1 1⟩ type in 3C, and the other grain oriented so that it also had a major vector aligned [17]. High-resolution images obtained under such conditions indicated that the amorphous films in the grain boundaries were of the order 0.5 to 1 nm. A typical example of the images obtained using these conditions is shown in Fig. 7. It is generally acknowledged that currently available analytical TEM techniques are not capable of chemically analysing at this level of film thickness, and microdiffraction techniques were not adequate.

3.2. Indentation response

The response to indentation of the two materials was predominantly the same; we shall therefore give a general description of the phenomenon, being specific where required. Two forms of fracture pattern were observed. Firstly, those associated with radial-type cracking [18], which emanated from the indent corners and were never seen to enter the zone beneath the indent. Secondly, the deformation zone directly beneath the indent. We shall describe each in turn. Lateral cracks [18] were not observed for the indenter loads used in this investigation.

On indentation of the as-polished samples the induced cracks did not completely propagate across the

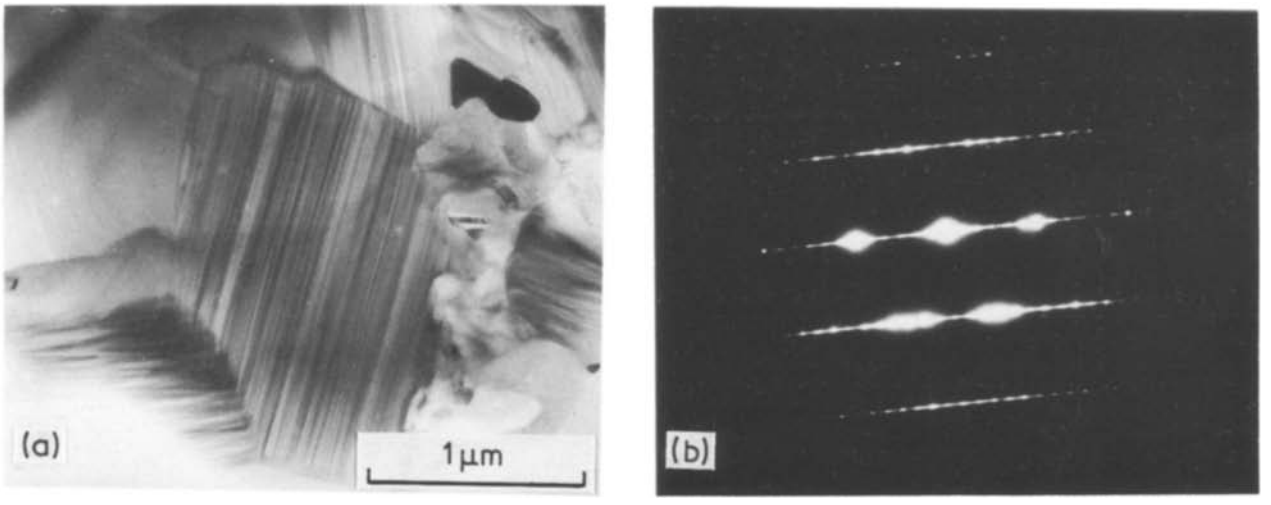

Figure 3 (a) Bright-field electron microscope image of a non-tabular grain in β-SiC and (b) electron diffraction pattern of the same grain showing 6H polytype.

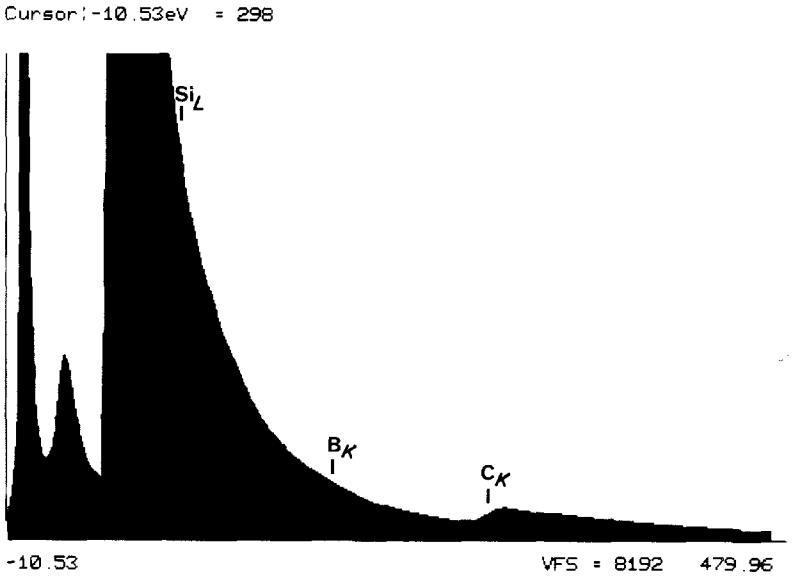

Figure 4 Electron energy-loss spectrum of the inclusion shown in Fig. 1. Positions of B_K, C_K and Si_L edges are indicated. Note that only the carbon edge is present.

50 μm spacing between the indents. After thinning to electron transparency, however, the cracks had completely joined up between the indents. This phenomenon allowed us to examine the crack propagation which occurred under two different circumstances: firstly rapid propagation after removal of the load, and secondly slow propagation as a result of residual stress relief during the ion-thinning process. Observations of these two different conditions showed that in both cases the radial cracks proceeded with minimal grain-boundary interaction. A very typical example is shown in Fig. 8, where the crack deflects only minimally when crossing a grain boundary and does not deviate significantly from its path to interact with boundaries. Note also that in this region the crack had the opportunity to follow grain boundaries but instead proceeded in a transgranular manner.

Cracks which entered grains at some small angle to a low-index plane occasionally switched direction to what would have been assumed an easier propagation path. When the cracks did change plane and direction they showed little crystallographic preference. Very often a crack would sweep through a grain and past a configuration which should have been a preferred fracture plane. At grain boundaries, crack inflections and boundary interactions were invariably observed, but unless a grain boundary was aligned relatively closely to the propagation path the crack did not follow it, preferring instead to take an intergranular path. When exceptions to the general transgranular fracture mode were observed they occurred most often at the tabular grain boundaries in the β-SiC material. Virtually no crack branching was observed and when it did, it occurred in regions where slow crack growth had taken place.

Careful inspection of smaller radial cracks and microcracks showed that an amorphous region was invariably seen to span the crack. These regions were identified from SAED ring patterns as carbon, and were thought to arise from the ion-thinning process. Sasaki *et al.* [19] have also observed an "amorphous substance" in their propagated cracks in chemical vapour deposited SiC and Si_3N_4 materials. The main consequence of these regions was that they gave an indication that the crack under investigation occurred in the bulk material, and not as a consequence of the post-specimen-handling process.

Deformation beneath the indentation could be described in terms of two separate forms of cracking and apparent regions of intense plastic deformation.

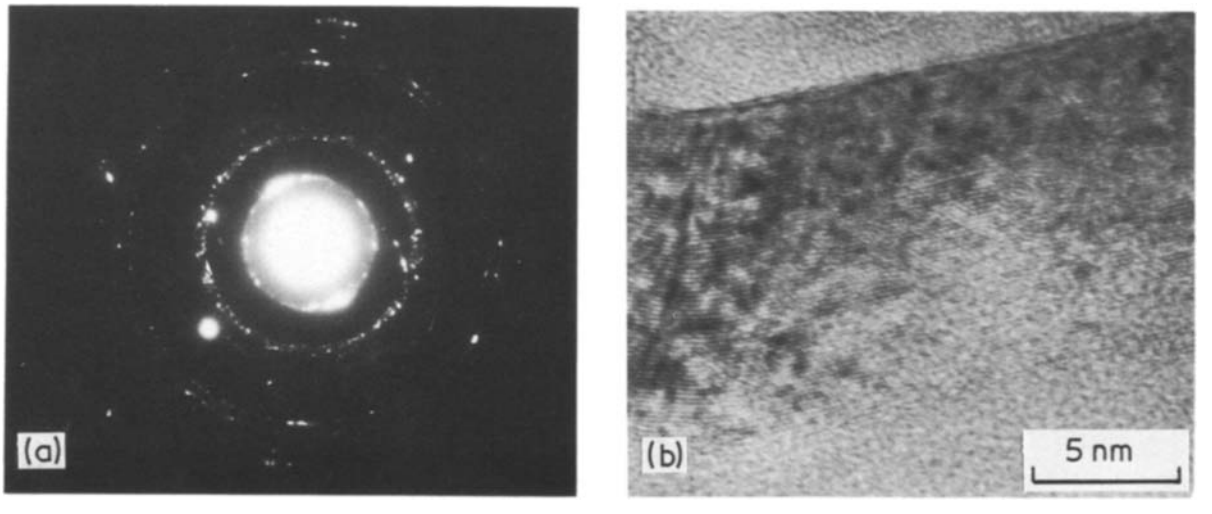

Figure 5 (a) SAED ring pattern of an inclusion in β-SiC, which can be indexed as graphite; (b) HREM showing graphite fringes.

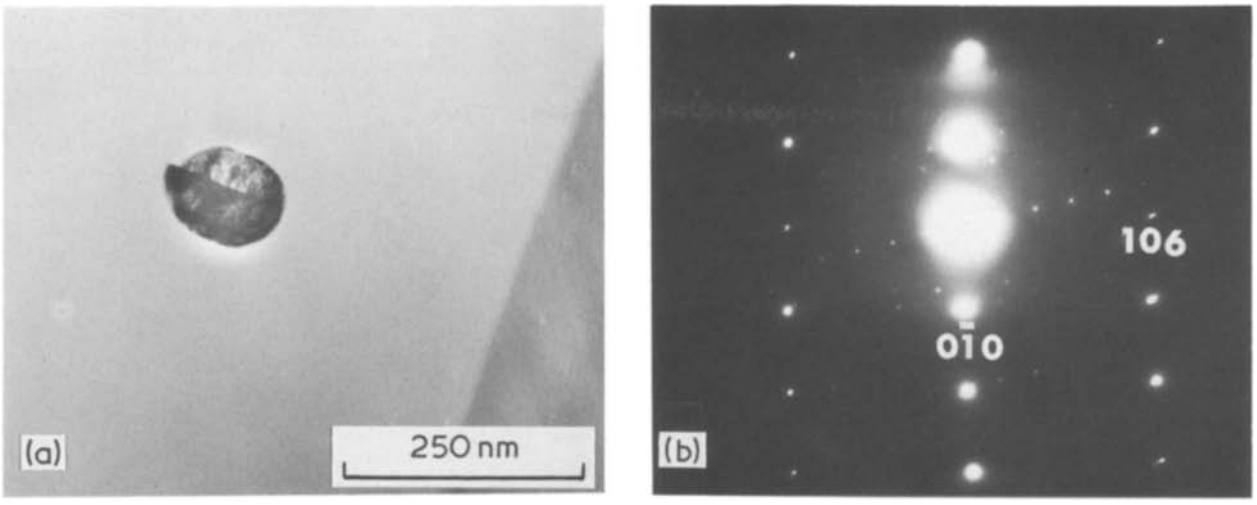

Figure 6 (a) Graphite inclusion within a β-SiC grain, (b) diffraction pattern, [6 0 $\bar{1}$] zone, from inclusion; weak spots are due to the matrix.

Firstly, cracks occurring parallel to the indented facet–sample surface contact region. Secondly, major and minor microcracks spanning these "facet" cracks. The microcracks generally occurred entirely within a grain and were aligned with generally preferred orientations to low-index directions. Fig. 9 shows the tip of a microcrack and it can be seen this crack has an approximate preferred orientation on (0 0 0 1). It is also evident from Fig. 9 that a craze zone extends beyond the crack tip, showing significant lattice distortion of the lattice around the tip, and that the crack is not atomically sharp at this point. At times two such matrix cracks would occur on a basal plane within the same grain but lie at about 60° to each other, indicating they preferred to lie on the α-axes in hexagonal notation. SAED patterns of the apex regions of indents, while still showing the matrix to be crystalline, exhibited very strong asterism indicative of strong directionality preference for the deformation beneath the various facets of the indenter. Such directionality was observed in adjacent grains when one grain was able to sustain the induced plastic deformation, while the adjacent grain introduced a crack from the grain boundary to accommodate the plastic strain (see Fig. 10). Such anisotropic plastic behaviour is typical for crystalline solids.

While direct evidence of discrete dislocation mobility was not observed under the indent, the severe deformation and faulting shown in Fig. 11 indicates the possible presence of very closely spaced pile-up dislocations (particularly in the arrowed regions). In such regions HREM lattice images were very difficult to obtain because of the large degree of deformation. Cracking was usually not observed within such heavily deformed regions. Dense dislocation tangles were observed just outside the indent profile; however, these regions were also too strained to perform diffraction contrast experiments. The bright- and dark-field electron microscope images of a "macro" area beneath an indent are shown in Figs 12a and b. The dark-field image (Fig. 12b) in particular shows the intense lattice distortion experienced by such regions.

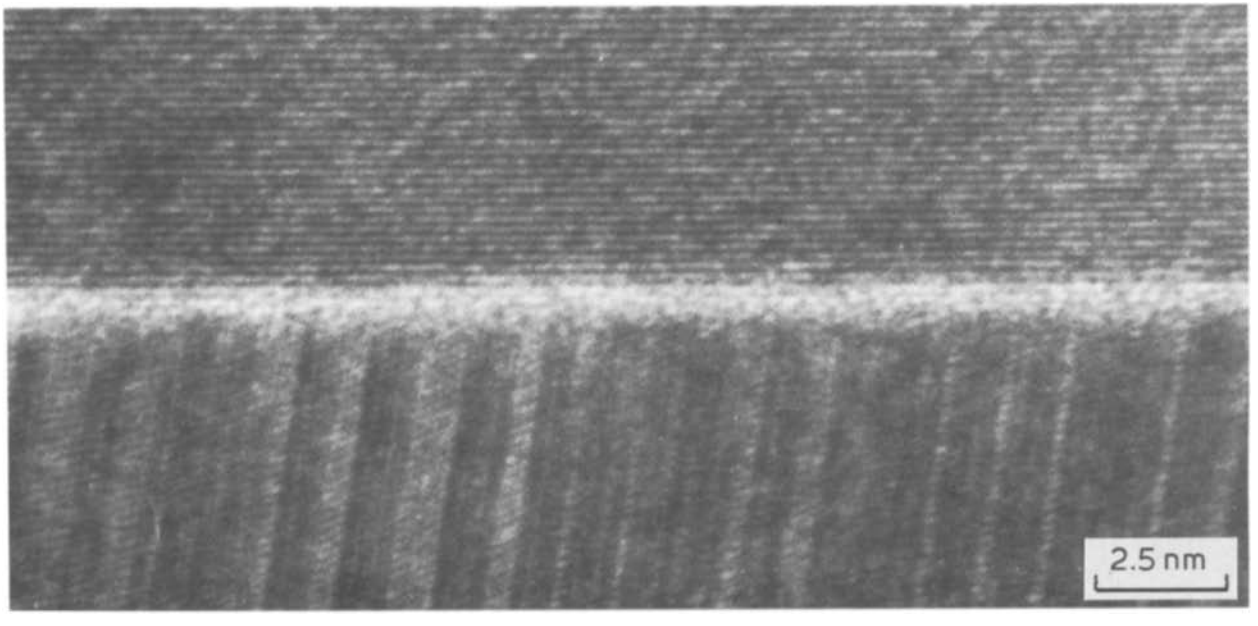

Figure 7 HREM image of a grain boundary in β-SiC, showing thin amorphous film between the grains.

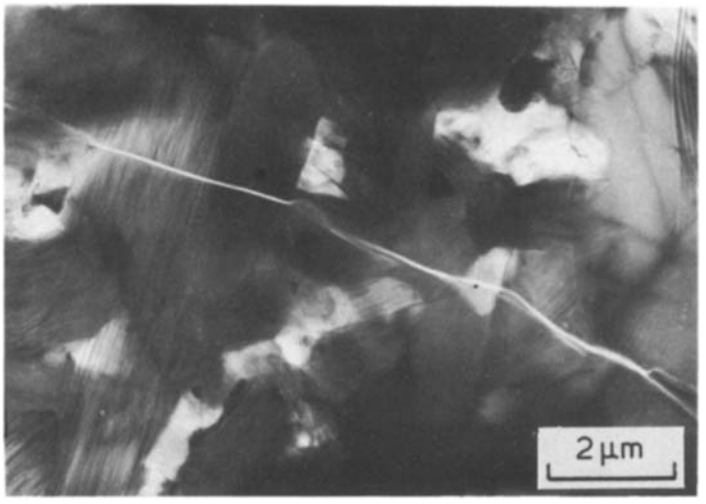

Figure 8 Radial-type crack propagation in β-SiC illustrating the lack of grain-boundary interaction.

4. Discussion

4.1. Microstructural aspects

Previous studies of pressureless-sintered SiC have reported significant porosity in such materials [9, 11, 13, 20]. As described in the previous section, our observations have shown that virtually all "pores" contained graphite, filling the pore volume in all cases to greater than 80%. As the carbon is a by-product of the fabrication process, its distribution may account for the large uniformly distributed "porosity" which is normally reported for these materials.

Porosity of this size, unless clustered, has in general very little effect on the strength of these materials, as a simple calculation using the Griffith equation and the values of Table I, with value of 450 GPa for E (corrected to the theoretical density) and $\sigma = (K_{Ic})^2/2E$, would show. Using these figures a critical crack size of about 14 μm is obtained. Therefore it is the grain size and not the porosity which is more likely to introduce the flaw which will be the strength-limiting factor for fracture initiation in these materials. The presence of the graphite in the pores accounts for virtually all the carbon used in our materials.

Spalin and Quinn [13] suggest that the carbon acts to retard grain growth. On the basis of the dissimilar grain sizes and morphologies in the two materials under investigation here, it is difficult to reconcile the role of graphite with grain refinement. If it were effective it would be more so in the α-SiC material where the grains grow with an approximate equiaxed morphology, rather than in the β-SiC material where the tabular grain morphology begins to dominate. Only rarely was the growth of tabular grains (growth of the long axis in the hexagonal a-axis direction) seen to be impeded by inclusions. The impediment to growth was generally another tabular grain, the graphite taking up the interstices between the grains.

The location of boron has to date eluded the present investigators. Previous work [9, 13] has suggested that boron selectively segregates to the grain boundaries. Another study [11], using signals from an electron microprobe, indicated that boron occurs as very large clusters. A different study which used electron microscopy [21] found the boron to be present as precipitates. We have used EELS to examine the inclusion regions but have failed to detect boron as clusters

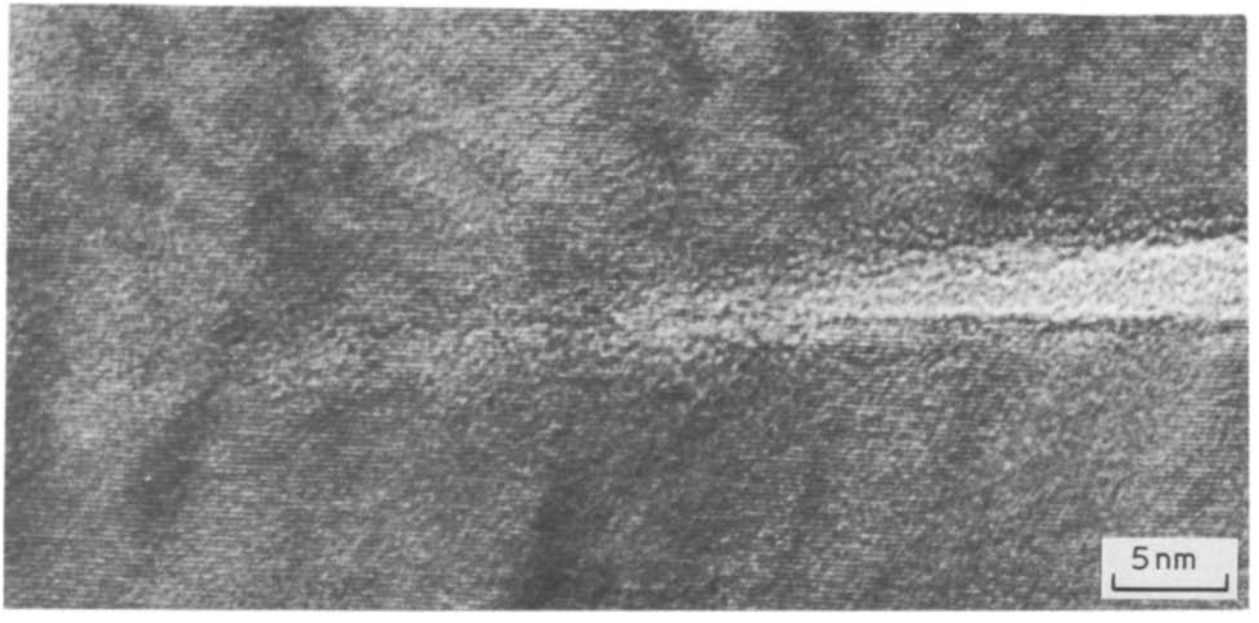

Figure 9 HREM image of a crack tip in the matrix from a region under the indentation. Note the apparent crazing and lack of planar crack propagation.

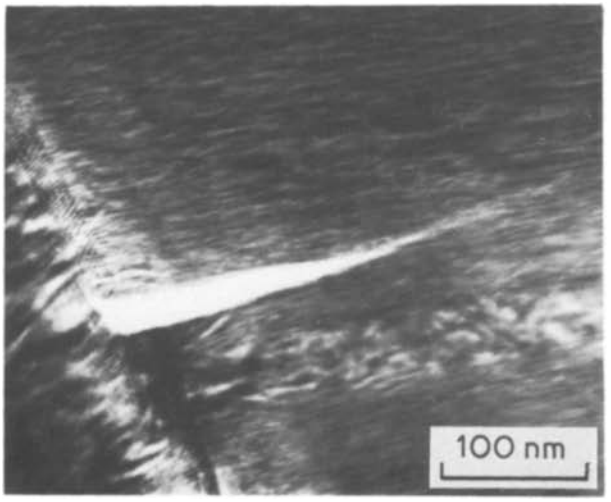

Figure 10 Microcrack initiated at a grain boundary. The adjacent grain has not cracked and was able to sustain the plastic strain imposed by the indenter.

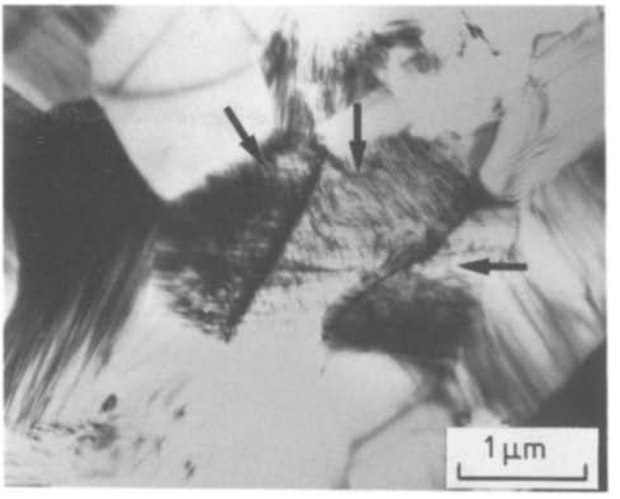

Figure 11 Region beneath the indenter showing fragmented grains and indicating the possible presence of closely spaced dislocations (arrowed) within these fragments.

(see Fig. 3) or inclusions. Grain boundaries were also examined, and as reported, amorphous boundary films, when detected, were of the order 0.5 to 1 nm thick. At this thickness film content analysis was not possible with the available technique. It has been suggested [22] that for SiC grains to bond with low-energy boundary configurations, dangling bonds at the surface of the grains must be occupied. If the grains are not to be joined by stacking faults or twins, it can be proposed that amorphous carbon, stabilized by the presence of boron, exists in the thin boundary layer. This method of joining can be considered similar to

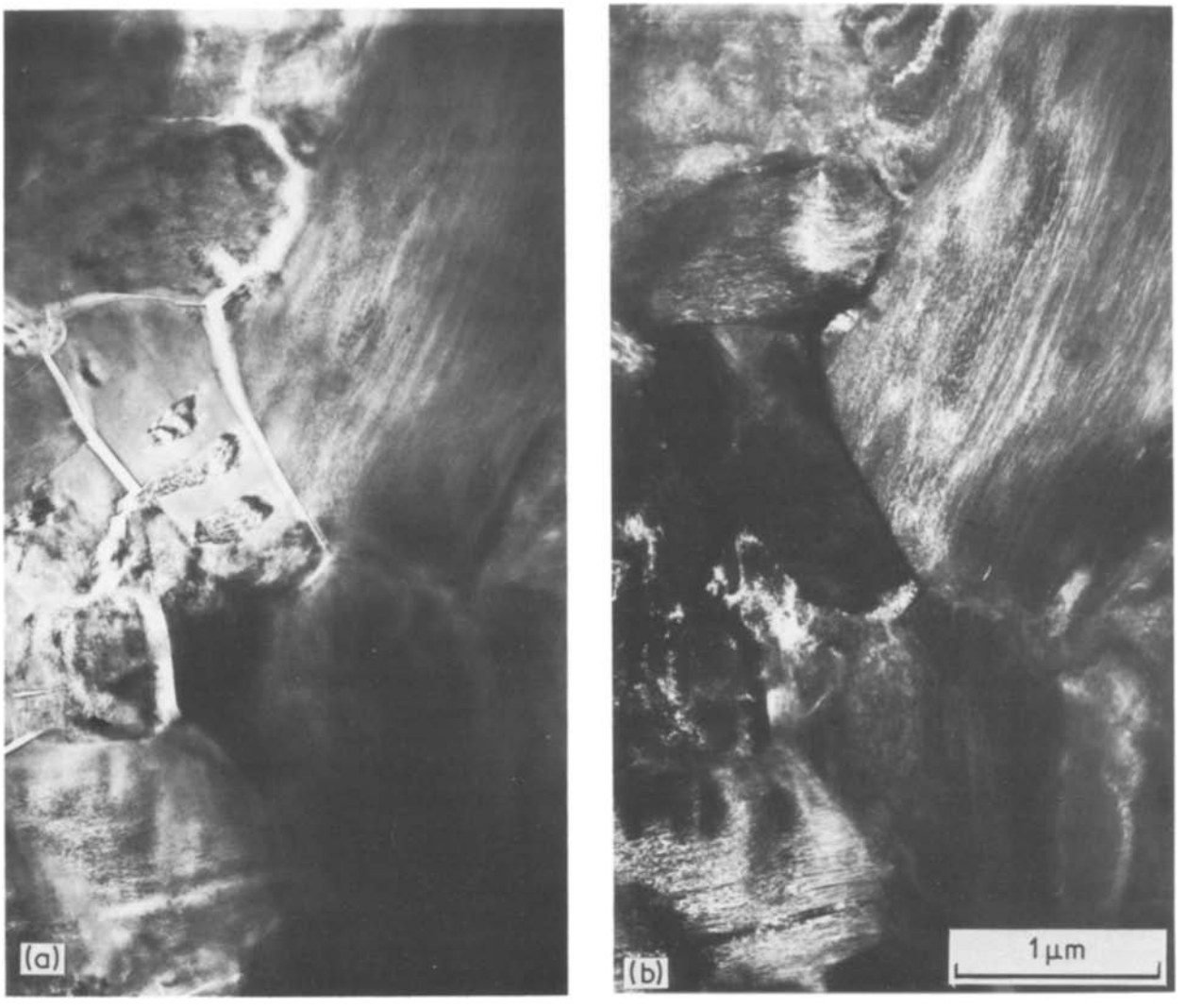

Figure 12 (a) Bright- and (b) dark-field electron microscope images of the general area of the intensely deformed zone beneath the indenter. Note the gross distortion of the faulting within the grains.

that which occurs in the joining of ionic oxide grains, where amorphous silica layers are present [23].

If the grains were joined by the incorporation of carbon and boron as an intermediate layer, such a layer would account for only a very small percentage of the boron. If all the boron were distributed around the grain boundaries as suggested [9], then at the levels used in these materials, 0.67 wt % ($\equiv$ 1.8 mol %) B, and an average grain size of about 6 μm, a film in excess of 30 nm would exist between any two grains. At this thickness the film and its composition would be readily detected. The solubility of boron in SiC at the firing temperature is reported to be about 0.2 mol % [24, 25]. This level is below the detection limit of boron using EELS. Thus the detection of solute boron within the grain could also not be analysed at these levels; equally, boron signals were not detected from clusters or precipitates either. Notwithstanding our observations it must be assumed that most of the boron is in pockets or precipitates as previously suggested [11, 21] and we have yet to locate them.

X-ray spectra of the β-SiC shows it to be almost entirely 3C, while SAED patterns of the same material indicates extensive α-polytypes as faults in the grains. A reconciliation of such results can best be made on the basis that the X-ray diffraction technique is not sensitive to the faulting which occurs within the grains. The occurrence of the faulting means that plastic deformation of these materials cannot be considered simply as that of cubic β-SiC. Interpretation becomes more complex because of the hexagonal and rhombohedral faulting. The β-SiC material can perhaps best be thought of an intermediate C–H or C–R crystal.

4.2. Indentation effects

The lack of preference for grain boundary fracture, in either fast or slow crack growth except at shallow angle impingement at tabular grain boundaries, is considered to be an indication of the clean state of the grain boundaries. Grain-boundary fracture occurs when the fracture energy of the boundary is significantly lower than that of the matrix. Page *et al.* [26], in their examination of the hardness and wear behaviour of hot-pressed SiC, observed intergranular fracture. They suggested that intergranular fracture may have occurred due to the presence of the hot-pressing additives, although this could not be confirmed with the microscope resolution available. The grain-boundary fracture in their material would be accentuated by the small grain size of their samples, which was 0.6 and 1.5 μm in a bimodal distribution.

From a fracture mechanics standpoint, while small grain sizes are desirable in reducing the critical flaw size they do little to enhance the fracture toughness. Claussen *et al.* [27] have observed that for alumina materials, increasing the grain size increased the toughness. This phenomenon can be attributed to two factors. Firstly, as the grain size is increased the propensity for intergranular fracture is increased, and secondly as a crack proceeds it will follow grain boundaries for short distances before turning back to the maximum tensile stress axis. This oscillation of the crack path has the effect of increasing the surface roughness, thereby increasing the surface fracture energy. Thus for the materials examined in this study the apparent lack of preference for intergranular fracture can be attributed to the clean grain boundaries, with the marginally better K_{Ic} for the β-SiC material (Table I) attributed to the larger grain size.

In a recent study of crack propagation in CVD-formed β-SiC, Niihara and Hirai [28] have shown that crack interaction with the faulting which occurred in their β-SiC can lead to a 33% increase in the material's K_{Ic} value. These workers have explained the increase in K_{Ic}, from ~ 3.8 to ~ 6 MPa m$^{1/2}$, due to crack interaction with the high fault density. Our observations have not found such intense interaction, even though the faulting in the β-SiC was very dense (e.g. Fig. 3a). While no explanation is immediately apparent, it may be that the modes of crack propagation in the two studies varied markedly.

The indentation plasticity and fracture which occur beneath indenters has been the subject of a number of studies (see for example [18, 30, 31]). It is generally agreed that plastic deformation, i.e. by the motion of dislocations, is possible in "brittle" materials in regions of high hydrostatic stress, such as are found beneath indenters. We have not observed individual dislocation activity directly below the indenter, but could surmise from image contrast that plastic flow involving dislocation activity had occurred (Fig. 11). Page *et al.* [26] observed dislocation motion in single-crystal α-SiC directly beneath the wear track of a sliding cone. These workers did not give Burgers vectors or slip planes for the observed dislocations. Our lack of observation may in part be the result of the polycrystalline nature of our specimens and the complex stress system which exists beneath Vickers indenters. A simpler indenter geometry of the Knoop type, which can be used to determine slip systems of orientated single crystals [29, 30], would have been better to study the initiation of plastic deformation behaviour.

5. Conclusions

A study has been made of the microstructure and indentation response of pressureless-sintered (0.67 wt % B and 2 wt % C doped) α- and β-SiC, using optical and high-resolution analytical electron microscopy. From the observations, the following conclusions could be made:

1. X-ray diffraction showed the sample bars to be predominantly the same as the starting powders, namely 6H and 3C polytypes for the α- and β-SiC samples, respectively.

2. Optical examination of un-etched surfaces revealed virtually no porosity but a large number of inclusions.

3. The inclusions, observable by optical microscopy, were analysed to contain carbon, as graphite, no other elements being detected.

4. Whilst a search was made for boron, no boron was detected as either grain-boundary films, precipitates or inclusions.

5. Grain-boundary films were amorphous, and

when detected were of the order 0.5 to 1 nm. At this thickness the boundary phase was too thin to analyse using the available techniques.

6. Grain morphology was similar to that previously reported for pressureless-sintered SiC materials, i.e. the α-type had approximately equiaxed grains and the β-type contained equiaxed with a large number of tabular grains, which have previously been designated as α-SiC.

7. X-ray diffraction showed the fabricated β-SiC sample to be almost entirely 3C polytype. Electron microscope examination, however, revealed that the sample contained dense 4H, 6H and 15R polytype faults within the grains. The faulting was so dense that from a deformation point of view the material could not be considered 3C, but at some intermediate state between the β- and α-polytypes.

8. Rapid and slow propagation of radial cracks emanating from the indent corners was almost completely transgranular, except when impinging at shallow angles at the grain boundaries. This was particularly so for tabular grains in the β-SiC material.

9. Plastic deformation within the indentation zone was assumed to have occurred by gross dislocation activity (although individual dislocations could not be clearly resolved in such regions), with cracking parallel to the indenter facet–sample surface intersection and crystallographically orientated microcracking between these parallel cracks.

Acknowledgements

The authors are grateful to Mr P. Birtles for assistance with the optical microscopy and thin foil preparation and Drs J. Drennan and M. Trigg for constructive criticism of the text. The present work was supported by the Ministry of International Trade and Industries under a contract for the Fine Ceramics Project. R.H.J.H. also acknowledges a Japanese Government Research Award from the Science and Technology Agency which made a visit to NIRIM possible.

References

1. E. GUGEL, in "Ceramics in Advanced Engineering Technologies", edited by H. Krockel, M. Merz and O. Van Der Biest (Reidel, Dorderecht, 1984) pp. 23–50.
2. R. A. ALLIEGRO, L. B. COFFIN and J. R. TINKELPAUGH, *J. Amer. Ceram. Soc.* **39** (1956) 386.
3. S. SOMIYA and S. SAITO (eds), Proceedings of International Symposium on Factors in Densification and Sintering of Oxide and Non-Oxide Ceramics, (Association of Science Document Information, Tokyo Institute of Technology, Tokyo, Japan, 1979).
4. W. BOCKER, H. LANDFERMONN and H. HAUSNER, *Powder Met. Int.* **11** (1979) 83.
5. M. OMORI and H. TAKEI, *Commun. Amer. Ceram. Soc.* **65** (1982) C-92.
6. S. PROCHASKA, General Electric Report, 73CRD325 (1973).
7. S. PROCHASKA and R. J. CHARLES, *Amer. Ceram. Soc. Bull.* **52** (1973) 885.
8. S. PROCHASKA and R. M. SCANLAN, General Electric Report 74CRD226 (1974).
9. S. PROCHASKA, "Special Ceramics 6" (British Ceramic Research Association, Stoke-on-Trent, 1975) p. 171.
10. E. GUGEL and G. LEINER, NATO AGARD Conference Proceedings No. 276, 1979, p. 276.
11. T. MIZRAH, M. HOFFMANN and L. GAUCKLER, *Powder Met. Int.* **16** (1984) 217.
12. H. TANAKA, Y. INOMATA, K. HARA and H. HASEGAWA, *J. Mater. Sci. Lett.* **4** (1985) 315.
13. M. J. SLAVIN and G. D. QUINN, *Int. J. High Tech. Ceram.* **3** (1987) 47.
14. G. ORANGE, H. TANAKA, and G. FANTOZZI, *Ceram. Int.* **13** (1987) 159.
15. C. A. JOHNSON, "Fracture Mechanics of Ceramics", Vol. 3 (Plenum, New York, 1978) p. 99.
16. A. P. SMITH, *Amer. Ceram. Soc. Bull.* **62** (1983) 886.
17. D. R. CLARKE, *J. Amer. Ceram. Soc.* **62** (1979) 236.
18. B. R. LAWN and M. V. SWAIN, *J. Mater. Sci.* **10** (1975) 113.
19. G. SASAKI, K. HIRAGA, M. HIRABAYASHI, K. NIIHARA and T. HIRAI, in Proceedings of 11th International Congress on Electron Microscopy, Kyoto (Japanese Society of Electron Microscopy, Tokyo, Japan, 1986) p. 1679.
20. H. TANAKA and Y. INOMATA, *J. Jpn Ceram. Soc.* **93** (1985) 450.
21. M. RUHLE and G. PETZOW, "Materials Science Research", Vol. 14 (Plenum, New York, 1981) p. 167.
22. Y. UEMURA, Y. INOMATA and Z. INOUE, *J. Mater. Sci.* **16** (1981) 2333.
23. D. R. CLARKE, *J. Amer. Ceram. Soc.* **70** (1987) 15.
24. P. T. B. SHAFFER, *Mater. Res. Bull.* **4** (1969) 213.
25. Y. A. VODAKOHOV and K. N. MOKHOV, in Proceedings of 3rd International Conference on SiC, Miami, Florida, September 1973 edited by R. C. Marshall, J. W. Faust Jr and C. E. Ryan (University of Southern Carolina Press, Columbia, S.C., 1974) p. 508.
26. T. F. PAGE, G. R. SAWYER, O. O. ADEWOYE and J. J. WERT, *Proc. Br. Ceram. Soc.* No. 26 (1978) 193.
27. N. CLAUSSEN, B. MUSSLER and M. V. SWAIN, *J. Amer. Ceram. Soc.* **65** (1983) C-14.
28. K. NIIHARA and T. HIRAI, *Bull. Ceram. Soc. Jpn* **21** (1986) 598 (in Japanese).
29. *Idem,* in Proceedings of Interfaces Conference, Berkeley, December 1986.
30. C. A. BROOKES, J. B. O'NEILL and B. A. W. REDFERN, *Proc. R. Soc.* **A322** (1971) 73.
31. P. J. BLAU and B. R. LAWN (eds.), "Microindentation Techniques in Materials Science and Engineering", ASTM Special Technical Publication No. 889 (American Society for Testing and Materials, Philadelphia, 1986).

Received 18 May
and accepted 22 July 1987